

Density estimation via mixture discrepancy and moments

Zhengyang Lei^a, Sihong Shao^a

^a*CAPT, LMAM and School of Mathematical Sciences, Peking University, Beijing 100871, China*

Abstract

With the aim of generalizing histogram statistics to higher dimensional cases, density estimation via discrepancy based sequential partition (DSP) has been proposed [D. Li, K. Yang, W. Wong, Advances in Neural Information Processing Systems (2016) 1099–1107] to learn an adaptive piecewise constant approximation defined on a binary sequential partition of the underlying domain, where the star discrepancy is adopted to measure the uniformity of particle distribution. However, the calculation of the star discrepancy is NP-hard and it does not satisfy the reflection invariance and rotation invariance either. To this end, we use the mixture discrepancy and the comparison of moments as a replacement of the star discrepancy, leading to the density estimation via mixture discrepancy based sequential partition (DSP-mix) and density estimation via moments based sequential partition (MSP), respectively. Both DSP-mix and MSP are computationally tractable and exhibit the reflection and rotation invariance. Numerical experiments in reconstructing the d -D mixture of Gaussians and Betas with $d = 2, 3, \dots, 6$ demonstrate that DSP-mix and MSP both run approximately ten times faster than DSP while maintaining the same accuracy.

Keywords: Density estimation; Adaptive sequential partition; Star discrepancy; Mixture discrepancy; Moment; Hausdorff moment problem; mixture of Gaussians; mixtures of Betas

1. Introduction

Density estimation is a classical problem in statistics and scientific computing. Given N independent and identically distributed observations $\mathbf{x}_1, \mathbf{x}_2, \dots, \mathbf{x}_N$, which follow the probability density $p(\mathbf{x})$. This paper focuses on how to estimate $p(\mathbf{x})$ from $\mathbf{x}_1, \mathbf{x}_2, \dots, \mathbf{x}_N$ via a nonparametric and adaptive domain partition approach. In nonparametric models, a widely used method is the kernel density estimation with the magic lying in how to balance the bias and variance of the estimator [1, 2]. Another simple and classical approach is the histogram statistics, a uniform piecewise constant density estimator. Due to the curse of dimensionality, it is difficult to apply the histogram to high-dimensional problems [3]. An adaptive nonparametric density estimation via Discrepancy based Sequential Partition (DSP) was proposed to reconstruct an adaptive piecewise constant approximation of $p(\mathbf{x})$ [4] and DSP is expected to handle higher dimensions [5]. DSP uses the star discrepancy, a concept from the quasi-Monte Carlo method, to measure the uniformity of the observations [6, 7]. When the star discrepancy of the observations within a sub-domain is small, it can be reasonable to think that their distribution approaches the uniform distribution and thus the corresponding probability density can be regarded as approximately constant in the sub-domain.

For a point set $(\mathbf{y}_1, \dots, \mathbf{y}_n) \subset [0, 1]^d$, its star discrepancy reads

$$D^*(\mathbf{y}_1, \dots, \mathbf{y}_n) = \sup_{\mathbf{u} \in [0, 1]^d} \left| \frac{1}{n} \sum_{i=1}^n \mathbb{1}_{[0, \mathbf{u}]}(\mathbf{y}_i) - \text{vol}([0, \mathbf{u}]) \right|, \quad (1)$$

Email addresses: leizy@stu.pku.edu.cn (Zhengyang Lei), sihong@math.pku.edu.cn (Sihong Shao)

and measures the uniformity of the points by using the infinity norm of the difference between the cumulative distribution function of the discrete point measure $\frac{1}{n} \sum_{i=1}^n \delta_{\mathbf{y}_i}$ and that of the uniform measure. Unfortunately, the star discrepancy possesses some drawbacks as follows [8].

- The star discrepancy is difficult to calculate: The calculation of the star discrepancy is NP-hard and requires the external approximate solver [9, 10]. When the sample size N is large, the calculation is rather time-consuming (As shown in Tables 4 and 5, DSP needs dozens of seconds for $N = 1 \times 10^6$);
- The star discrepancy does not satisfy reflection invariance [8, 11]: The point sets in Figures 1(a) and 1(b) are symmetric about the line $x_1 = 0.5$, but the values of their star discrepancies are not equal, which is counterintuitive. The reason for this phenomenon lies in the fact that the origin $\mathbf{0}$ is distinctive in the definition of the star discrepancy;
- The star discrepancy does not satisfy rotation invariance [8, 11]: Figure 2(b) is obtained by rotating Figure 2(a) 90 degrees clockwise, and the value of the star discrepancy changes after the rotation. The reason for this phenomenon is also that the origin $\mathbf{0}$ is distinctive in the definition of the star discrepancy.

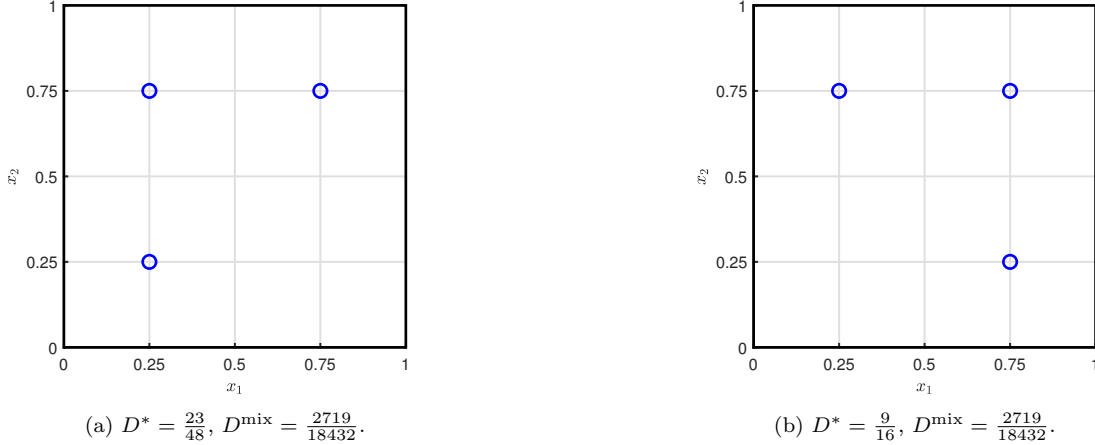


Figure 1. Reflection invariance test, $d = 2, N = 3$: Figures 1(a) and 1(b) are symmetric about $x_1 = 0.5$. Intuitively, the reflection transformation should not change the uniformity of points. However, the star discrepancies of Figures 1(a) and 1(b) are different.

In view of the drawbacks of the star discrepancy, this paper contributes two new uniformity measurement strategies for density estimation.

- One is the mixture discrepancy, another kind of discrepancy. For a point set $(\mathbf{y}_1, \dots, \mathbf{y}_n) \subset [0, 1]^d$, its mixture discrepancy has an analytical expression,

$$\begin{aligned}
 & D^{\text{mix}}((\mathbf{y}_1, \dots, \mathbf{y}_n))^2 \\
 &= \left(\frac{19}{12}\right)^d - \frac{2}{n} \sum_{i=1}^n \prod_{j=1}^d \left(\frac{5}{3} - \frac{1}{4} \left| y_{ij} - \frac{1}{2} \right| - \frac{1}{4} \left| y_{ij} - \frac{1}{2} \right|^2 \right) \\
 &+ \frac{1}{n^2} \sum_{i=1}^n \sum_{k=1}^n \prod_{j=1}^d \left(\frac{15}{8} - \frac{1}{4} \left| y_{ij} - \frac{1}{2} \right| - \frac{1}{4} \left| y_{kj} - \frac{1}{2} \right| - \frac{3}{4} |y_{ij} - y_{kj}| + \frac{1}{2} |y_{ij} - y_{kj}|^2 \right),
 \end{aligned} \tag{2}$$

where $\mathbf{y}_i = (y_{i1}, \dots, y_{id})$. It is thus easy to calculate, and possesses good theoretical properties. We use the same algorithm framework as DSP except for replacing the star discrepancy with the mixture discrepancy. The resulting method is dubbed the DSP-mix method;

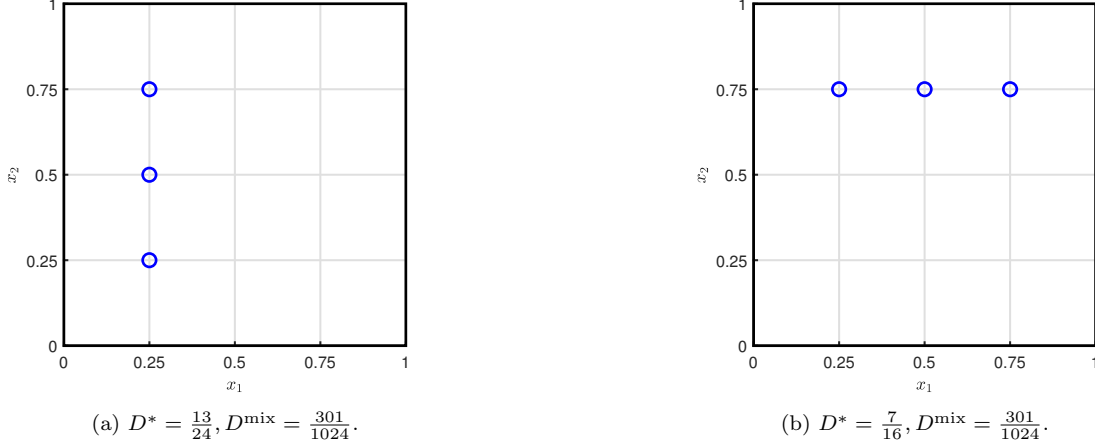


Figure 2. Rotation invariance test, $d = 2, N = 3$: Figure 2(b) is obtained by rotating Figure 2(a) 90 degrees clockwise. Intuitively, rotation should not change the uniformity of the points. However, the star discrepancies of Figure 2(a) and 2(b) are different.

- The other is the density estimation via moments based sequential partition (MSP), which still adopts the partitioning framework in DSP, but the way to measure the uniformity of the observations is changed to compare the gap between the moments of the particles and the moments of the uniform density.

Whether the density function can be uniquely determined by the moments of all orders is the classical moment problem in probability theory [12, 13, 14]. For the case where the probability density is defined on a compact set, this problem is called the Hausdorff moment problem, and the answer is positive [15]. When the moments of all orders of the observations on the compact set are close to those of the uniform distribution, we can consider that the observations are approximately uniformly distributed. MSP is easy to calculate and satisfies the reflection and rotation invariance. Numerical experiments demonstrate that both DSP-mix and MSP achieve about ten times acceleration compared with DSP while maintaining the same accuracy.

The rest of this paper is organized as follows. The DSP-mix and MSP methods are introduced in Sections 2 and 3, respectively. Section 4 conducts several numerical experiments and compares DSP-mix and MSP with DSP in performance. The paper is concluded in Section 5.

2. The DSP-mix method

DSP uses an adaptive piecewise constant density estimator to reconstruct the d -D probability density function from the observations [4]. DSP-mix inherits the algorithm framework of DSP and only differs in the measure of uniformity. Without loss of generality, assume that the observations $\mathbf{x}_i \in \Omega = [0, 1]^d, i = 1, 2, \dots, N$, and the computational domain Ω is decomposed into L subdomains,

$$\Omega = \bigcup_{l=1}^L \Omega_l. \quad (3)$$

DSP-mix tries to approximate the density function $p(\mathbf{x})$ with a piecewise constant function,

$$\hat{p}(\mathbf{x}) = \sum_{l=1}^L c_l \mathbb{1}_{\Omega_l}(\mathbf{x}), \quad (4)$$

where

$$c_l = \frac{1}{N|\Omega_l|} \sum_{i=1}^N \mathbb{1}_{\Omega_l}(\mathbf{x}_i). \quad (5)$$

To be more specific, DSP-mix adopts a sequential binary partitioning strategy to obtain the decomposition (3) during which the mixture discrepancy is adopted to measure the uniformity. When the mixture discrepancy of the observations within the sub-domain Ω_l is less than a predetermined threshold, it can be approximately considered that the observations within this sub-domain are uniformly distributed, and the corresponding density function can be approximated as a constant. Algorithm 1 presents the detailed process. It can be readily seen there that if there exists a sub-domain Ω_l fails to pass the uniformity test (See Lines 7-14), then Ω_l is split along a certain coordinate and two new sub-domains, $\Omega_l^{(1)}$ and $\Omega_l^{(2)}$, are generated. Subsequently, these two newly generated sub-domains are combined with the remaining sub-domains to update the sub-domain set \mathcal{P}_{L+1} (see Line 17).

Algorithm 1 The DSP-mix method.

Input: The domain Ω , particle set \mathbf{x}_i , $i = 1, 2, \dots, N$, parameters θ, m .
Output: An adaptive piecewise constant approximation of probability density function $p(\mathbf{x})$.

- 1: $L = 1, \Omega_1 = \Omega, \mathcal{P}_1 = \{\Omega_1\}$;
- 2: **while** true **do**
- 3: flag = 0;
- 4: **for all** $\Omega_l = \prod_{j=1}^d [a_j^{(l)}, b_j^{(l)}] \in \mathcal{P}_L$ **do**
- 5: Denote $S_l = \{(y_{i1}^{(l)}, \dots, y_{id}^{(l)})\}_{i=1}^n$ as the subset of particles that fall within Ω_l and $n = |S_l|$;
- 6: Measure the uniformity of S_l ;
- 7: **if** S_l cannot be approximated as a uniform distribution **then**
- 8: $L \leftarrow L + 1$;
- 9: Choose a splitting node $\tilde{s}_{i_0, j_0}^{(l)}$ according to Eq. (6);
- 10: Divide Ω_l into $\Omega_l^{(1)} \cup \Omega_l^{(2)}$ as Eq. (7);
- 11: $\Omega_l \leftarrow \Omega_l^{(1)}, \Omega_{L+1} \leftarrow \Omega_l^{(2)}$;
- 12: flag = 1;
- 13: Break;
- 14: **end if**
- 15: **end for**
- 16: **if** flag = 1 **then**
- 17: $\mathcal{P}_{L+1} \leftarrow \{\Omega_1, \dots, \Omega_{L+1}\}$;
- 18: **else**
- 19: Break;
- 20: **end if**
- 21: **end while**
- 22: Calculate piecewise constants c_l , $l = 1 \dots, L$ according to Eq. (5) and partition \mathcal{P}_L ;

Suppose $\Omega_l = \prod_{j=1}^d [a_j^{(l)}, b_j^{(l)}]$ and $S_l = \{(y_{i1}^{(l)}, \dots, y_{id}^{(l)})\}_{i=1}^n$ to be the subset of particles that fall within Ω_l . Two key issues are left to be specified in Algorithm 1: Where to split and whether to split.

- Where to split: We adopt $m - 1$ dividing points along each coordinate, and choose the uniformly distributed points for simplicity: $s_{i_0, j_0}^{(l)} = a_{j_0}^{(l)} + \frac{i_0}{m} (b_{j_0}^{(l)} - a_{j_0}^{(l)})$ with $i_0 = 1, 2, \dots, m - 1$

1 and $j_0 = 1, 2, \dots, d$. Accordingly, DSP-mix splits Ω_l using the dividing point $\tilde{s}_{i_0, j_0}^{(l)}$ that divides Ω_l into $\Omega_l^{(1)}$ and $\Omega_l^{(2)}$. Here $\tilde{s}_{i_0, j_0}^{(l)}$ is selected according to

$$\tilde{s}_{i_0, j_0}^{(l)} = \arg \max_{s_{i_0, j_0}^{(l)}} \left| \frac{n_{i_0, j_0}}{n} - \frac{i_0}{m} \right|, \quad (6)$$

where n_{i_0, j_0} count the number of particles in S_l that fall within $\Omega_l^{(1)}$, and

$$\begin{aligned} \Omega_l^{(1)} &= \prod_{j=1}^{j_0-1} [a_j^{(l)}, b_j^{(l)}] \times [a_{j_0}^{(l)}, s_{i_0, j_0}^{(l)}] \times \prod_{j=j_0+1}^d [a_j^{(l)}, b_j^{(l)}], \\ \Omega_l^{(2)} &= \Omega_l \setminus \Omega_l^{(1)}. \end{aligned} \quad (7)$$

The intuition behind Eq. (6) is to find the most non-uniform sub-domain $\Omega_l^{(1)}$ for a given set of dividing points $\{s_{i_0, j_0}^{(l)} \mid i_0 = 1, 2, \dots, m-1, j_0 = 1, 2, \dots, d\}$;

- Whether to split: The linear scaling $\Omega_l \rightarrow [0, 1]^d$ is performed first before using the discrepancy as the uniformity measurement. We scale S_l to $\tilde{S}_l = \{(y_{i1}^{(l)} - a_1^{(l)})/b_1^{(l)}, \dots, (y_{id}^{(l)} - a_d^{(l)})/b_d^{(l)}\}_{i=1}^n$. The partitioning terminates when the mixture discrepancy of particles that fall within Ω_l satisfying

$$D^{\text{mix}}(\tilde{S}_l) \leq \frac{\theta \sqrt{N}}{n}. \quad (8)$$

DSP-mix uses the mixture discrepancy $D^{\text{mix}}(\tilde{S}_l)$ to measure the uniformity of S_l in Line 6 of Algorithm 1, while DSP uses the star discrepancy $D^*(\tilde{S}_l)$ instead. In Line 7 of Algorithm 1, DSP-mix considers S_l inapproximable as a uniform distribution when $D^{\text{mix}}(\tilde{S}_l) > \frac{\theta \sqrt{N}}{n}$, while DSP holds the same for $D^*(\tilde{S}_l) > \frac{\theta \sqrt{N}}{n}$. The parameter θ governs the depth of partition. The smaller θ is, the finer the partitioning it induces.

Compared with the star discrepancy adopted in DSP, the mixture discrepancy used in DSP-mix has the following advantages [11].

- Easy to calculate: The mixture discrepancy can be accurately calculated with a computational complexity of $\mathcal{O}(n^2 d)$ and thus any external solver is not required. Hence DSP-mix is expected to handle the density estimation problems more efficiently than DSP. In [16], DSP-mix is used to efficiently reconstruct the values of the Coulomb collision term from particles;
- Reflection invariance: The mixture discrepancy satisfies the reflection invariance [11]. Suppose that $(\tilde{\mathbf{y}}_1, \dots, \tilde{\mathbf{y}}_n)$ is the points obtained by reflecting $(\mathbf{y}_1, \dots, \mathbf{y}_n)$ about the plane $y_{j_0} = 1/2$, then

$$\tilde{\mathbf{y}}_i = (y_{i1}, \dots, y_{i, j_0-1}, 1 - y_{i, j_0}, y_{i, j_0+1}, \dots, y_{id}), \quad i = 1 \dots, n, \quad (9)$$

and

$$\begin{aligned}
& D^{\text{mix}}((\tilde{\mathbf{y}}_1, \dots, \tilde{\mathbf{y}}_n))^2 \\
&= \left(\frac{19}{12} \right)^d - \frac{2}{n} \sum_{i=1}^n \left(\frac{5}{3} - \frac{1}{4} \left| \frac{1}{2} - y_{i,j_0} \right| - \frac{1}{4} \left| \frac{1}{2} - y_{i,i_0} \right| \right) \prod_{j \neq j_0} \left(\frac{5}{3} - \frac{1}{4} \left| y_{ij} - \frac{1}{2} \right| - \frac{1}{4} \left| y_{ij} - \frac{1}{2} \right|^2 \right) \\
&\quad + \frac{1}{n^2} \sum_{i=1}^n \sum_{k=1}^n \left(\frac{15}{8} - \frac{1}{4} \left| \frac{1}{2} - y_{i,j_0} \right| - \frac{1}{4} \left| \frac{1}{2} - y_{k,j_0} \right| - \frac{3}{4} |y_{i,j_0} - y_{k,j_0}| + \frac{1}{2} |y_{i,j_0} - y_{k,j_0}|^2 \right) \\
&\quad \prod_{j \neq j_0} \left(\frac{15}{8} - \frac{1}{4} \left| y_{ij} - \frac{1}{2} \right| - \frac{1}{4} \left| y_{kj} - \frac{1}{2} \right| - \frac{3}{4} |y_{ij} - y_{kj}| + \frac{1}{2} |y_{ij} - y_{kj}|^2 \right) \\
&= D^{\text{mix}}((\mathbf{y}_1, \dots, \mathbf{y}_n))^2.
\end{aligned} \tag{10}$$

For the two point sets in Figures 1(a) and 1(b), their mixture discrepancies are both $\frac{2719}{18432}$;

- **Rotation invariance:** The mixture discrepancy satisfies the rotation invariance [11]. Suppose that $(\tilde{\mathbf{y}}_1, \dots, \tilde{\mathbf{y}}_n)$ is the points obtained by rotating $(\mathbf{y}_1, \dots, \mathbf{y}_n)$ 90 degrees clockwise about the $y_{i_0} - y_{j_0}$ plane, then for $\forall i = 1, \dots, n$,

$$\tilde{y}_{ij} = \begin{cases} y_{ij}, & j \neq i_0 \text{ and } j \neq j_0, \\ \cos(-\pi/2)(y_{i,i_0} - 0.5) - \sin(-\pi/2)(y_{i,j_0} - 0.5) + 0.5 = y_{i,j_0}, & j = i_0, \\ \sin(-\pi/2)(y_{i,i_0} - 0.5) + \cos(-\pi/2)(y_{i,j_0} - 0.5) + 0.5 = 1 - y_{i,i_0}, & j = j_0, \end{cases}$$

and it can be easily proved that $D^{\text{mix}}((\tilde{\mathbf{y}}_1, \dots, \tilde{\mathbf{y}}_n))^2 = D^{\text{mix}}((\mathbf{y}_1, \dots, \mathbf{y}_n))^2$, analogous to Eq.(10). For the two point sets in Figures 2(a) and 2(b), their mixture discrepancies are both $\frac{301}{1024}$.

3. The MSP method

MSP still adopts the framework of Algorithm 1. However, instead of using the discrepancy as the uniformity measurement, it judges whether the particle set S_l in Ω_l is close to a uniform distribution by comparing whether the moments of the discrete point measure $\frac{1}{n} \sum_{i=1}^n \delta_{\mathbf{y}_i}$ and the uniform measure are near enough. Suppose that the d -dimensional random variable $\mathbf{y} = (y_1, y_2, \dots, y_d)$ follows the probability density $q(\mathbf{y})$, the d -dimensional index $\mathbf{k} = (k_1, k_2, \dots, k_d)$, $\mathbf{y}^{\mathbf{k}} = y_1^{k_1} y_2^{k_2} \dots y_d^{k_d}$, $\mathbb{N}_0 = \{0, 1, 2, \dots\}$, then the moment of order $|\mathbf{k}| = \sum_{i=1}^d k_i$ of the probability density $q(\mathbf{y})$ is defined as

$$m_{\mathbf{k}}(q) = \int_{\mathbb{R}^d} \mathbf{y}^{\mathbf{k}} q(\mathbf{y}) d\mathbf{y}, \quad \mathbf{k} \in \mathbb{N}_0^d. \tag{11}$$

We call $\{m_{\mathbf{k}}(q), \mathbf{k} \in \mathbb{N}_0^d\}$ the moment sequence. Whether the probability density on a compact set can be uniquely determined by the moment sequence is the Hausdorff moment problem in probability theory, and its answer is positive [15].

Theorem 3.1. ([15]) *The probability density function defined on a compact set is uniquely determined by its moment sequence.*

For two probability densities defined on a compact set, we can judge whether they are close by comparing their moment sequences. In actual numerical implementation, we discover that conducting comparisons up to the order of $|\mathbf{k}| \leq 2$ is capable of attaining satisfactory numerical effects, that is, only the expectation and the covariance matrix are considered. Denote the expectation of the uniform measure on the sub-domain Ω_l as $\boldsymbol{\mu}^{(l)} = (\mu_1^{(l)}, \dots, \mu_d^{(l)}) \in \mathbb{R}^d$, and the covariance matrix as

$\Sigma^{(l)} = (\Sigma_{ij}^{(l)}) \in \mathbb{R}^{d \times d}$. The expectation of the particle subset S_l is $\hat{\boldsymbol{\mu}}^{(l)} = (\hat{\mu}_1^{(l)}, \dots, \hat{\mu}_d^{(l)}) \in \mathbb{R}^d$, and the covariance matrix is $\hat{\Sigma}^{(l)} = (\hat{\Sigma}_{ij}^{(l)}) \in \mathbb{R}^{d \times d}$. They have the explicit calculation expressions,

$$\begin{aligned}
\mu_j^{(l)} &= \frac{a_j^{(l)} + b_j^{(l)}}{2}, \quad j = 1, \dots, d, \\
\Sigma_{jj}^{(l)} &= \frac{(b_j^{(l)} - a_j^{(l)})^2}{12}, \quad j = 1, \dots, d, \\
\Sigma_{ij}^{(l)} &= 0, \quad i \neq j, \\
\hat{\boldsymbol{\mu}}^{(l)} &= \frac{1}{n} \sum_{i=1}^n \mathbf{y}_i^{(l)}, \\
\hat{\Sigma}^{(l)} &= \frac{1}{n} \sum_{i=1}^n (\mathbf{y}_i^{(l)} - \hat{\boldsymbol{\mu}}^{(l)}) (\mathbf{y}_i^{(l)} - \hat{\boldsymbol{\mu}}^{(l)})^T.
\end{aligned} \tag{12}$$

MSP runs the uniformity test as follows

$$\begin{aligned}
|\mu_j^{(l)} - \hat{\mu}_j^{(l)}| &< \epsilon_1 (b_j^{(l)} - a_j^{(l)}), \quad j = 1, \dots, d, \\
|\Sigma_{jj}^{(l)} - \hat{\Sigma}_{jj}^{(l)}| &< \epsilon_2 |\Sigma_{jj}^{(l)}|, \quad j = 1, \dots, d, \\
|\hat{\Sigma}_{ij}^{(l)}| &< \epsilon_3, \quad i \neq j,
\end{aligned} \tag{13}$$

where $\epsilon_1, \epsilon_2, \epsilon_3 > 0$ are tolerance parameters. If Eq. (13) is satisfied, MSP terminates the sequential partition; Otherwise we consider that S_l cannot be approximated as the uniform distribution in Line 7 of Algorithm 1. Obviously, MSP has the following advantages over DSP.

- Easy to calculate: The computational complexity of the expectation is $\mathcal{O}(nd)$, and the computational complexity of the covariance matrix is $\mathcal{O}(nd^2)$. Both of them are linear functions of the number of particles n ;
- Reflection invariance: Suppose that $(\tilde{\mathbf{y}}_1, \dots, \tilde{\mathbf{y}}_n)$ is the points obtained by reflecting $(\mathbf{y}_1, \dots, \mathbf{y}_n)$ about the plane $y_{j_0} = \frac{a_{j_0}^{(l)} + b_{j_0}^{(l)}}{2}$, then

$$\tilde{\mathbf{y}}_i = \left(y_{i1}, \dots, y_{i,j_0-1}, a_{j_0}^{(l)} + b_{j_0}^{(l)} - y_{i,j_0}, y_{i,j_0+1}, \dots, y_{id} \right), \quad i = 1 \dots, n. \tag{14}$$

Let $\tilde{\boldsymbol{\mu}}^{(l)} = \frac{1}{n} \sum_{i=1}^n \tilde{\mathbf{y}}_i^{(l)}$ and $\tilde{\Sigma}^{(l)} = \frac{1}{n} \sum_{i=1}^n (\tilde{\mathbf{y}}_i^{(l)} - \tilde{\boldsymbol{\mu}}^{(l)}) (\tilde{\mathbf{y}}_i^{(l)} - \tilde{\boldsymbol{\mu}}^{(l)})^T$, then

$$\left| \mu_j^{(l)} - \tilde{\mu}_j^{(l)} \right| = \begin{cases} \left| \mu_j^{(l)} - \hat{\mu}_j^{(l)} \right|, & j \neq j_0, \\ \left| \frac{a_j^{(l)} + b_j^{(l)}}{2} - (a_j^{(l)} + b_j^{(l)}) + \hat{\mu}_j^{(l)} \right| = \left| \mu_j^{(l)} - \hat{\mu}_j^{(l)} \right|, & j = j_0. \end{cases} \tag{15}$$

For $j \neq j_0$, it is obvious that $\left| \Sigma_{jj}^{(l)} - \widetilde{\Sigma}_{jj}^{(l)} \right| = \left| \Sigma_{jj}^{(l)} - \widehat{\Sigma}_{jj}^{(l)} \right|$. For $j = j_0$, we have

$$\begin{aligned}
& \left| \Sigma_{j_0 j_0}^{(l)} - \widetilde{\Sigma}_{j_0 j_0}^{(l)} \right| \\
&= \left| \Sigma_{j_0 j_0}^{(l)} - \frac{1}{n} \sum_{i=1}^n \left(a_{j_0}^{(l)} + b_{j_0}^{(l)} - y_{i,j_0} - \frac{1}{n} \sum_{k=1}^n (a_{j_0}^{(l)} + b_{j_0}^{(l)} - y_{k,j_0}) \right)^2 \right| \\
&= \left| \Sigma_{j_0 j_0}^{(l)} - \frac{1}{n} \sum_{k=1}^n \left(y_{i,j_0} - \frac{1}{n} \sum_{k=1}^n y_{k,j_0} \right)^2 \right| \\
&= \left| \Sigma_{j_0 j_0}^{(l)} - \widehat{\Sigma}_{j_0 j_0}^{(l)} \right|.
\end{aligned} \tag{16}$$

For $i \neq j_0$, $j \neq j_0$ and $i \neq j$, it is patently clear that $\left| \widetilde{\Sigma}_{ij}^{(l)} \right| = \left| \widehat{\Sigma}_{ij}^{(l)} \right|$. When $i \neq j_0$ and $j = j_0$,

$$\begin{aligned}
& \left| \widetilde{\Sigma}_{i j_0}^{(l)} \right| \\
&= \left| \frac{1}{n} \sum_{k=1}^n \left(y_{k,i} - \frac{1}{n} \sum_{h=1}^n y_{h,i} \right) \left(a_{j_0}^{(l)} + b_{j_0}^{(l)} - y_{k,j_0} - \frac{1}{n} \sum_{h=1}^n (a_{j_0}^{(l)} + b_{j_0}^{(l)} - y_{h,j_0}) \right) \right| \\
&= \left| \frac{1}{n} \sum_{k=1}^n - \left(y_{k,i} - \frac{1}{n} \sum_{h=1}^n y_{h,i} \right) \left(y_{k,j_0} - \frac{1}{n} \sum_{h=1}^n y_{h,j_0} \right) \right| \\
&= \left| \widehat{\Sigma}_{ij}^{(l)} \right|.
\end{aligned} \tag{17}$$

The situation with $i = j_0$ and $j \neq j_0$ is analogous. Combining Eqs. (15), (16) and (17) together, the reflection transformation has no impact on the termination criterion (13). For Figures 1(a) and 1(b), the differences between the expectations and covariance matrices of the two groups of particles and those of the uniform measure are

$$\begin{aligned}
\left| \boldsymbol{\mu}^{(l)} - \widehat{\boldsymbol{\mu}}^{(l)} \right| &= \left(\frac{1}{12}, \frac{1}{12} \right), \\
\left| \boldsymbol{\Sigma}^{(l)} - \widehat{\boldsymbol{\Sigma}}^{(l)} \right| &= \begin{pmatrix} \frac{1}{48} & \frac{1}{48} \\ \frac{1}{48} & \frac{1}{48} \end{pmatrix}.
\end{aligned} \tag{18}$$

where the absolute is performed element-wise;

- Rotation invariance: Suppose that $(\widetilde{\boldsymbol{y}}_1, \dots, \widetilde{\boldsymbol{y}}_n)$ is the points obtained by rotating $(\boldsymbol{y}_1, \dots, \boldsymbol{y}_n)$ 90 degrees clockwise about the $y_{i_0} - y_{j_0}$ plane with the center of Ω_l as the center of rotation, then for $\forall i = 1, \dots, n$,

$$\begin{aligned}
& \widetilde{y}_{i i_0} \\
&= \cos \left(-\frac{\pi}{2} \right) \left(y_{i, i_0} - \frac{a_{i_0}^{(l)} + b_{i_0}^{(l)}}{2} \right) - \sin \left(-\frac{\pi}{2} \right) \left(y_{i, j_0} - \frac{a_{j_0}^{(l)} + b_{j_0}^{(l)}}{2} \right) + \frac{a_{j_0}^{(l)} + b_{j_0}^{(l)}}{2} \\
&= y_{i, j_0}, \\
& \widetilde{y}_{i j_0} \\
&= \sin \left(-\frac{\pi}{2} \right) \left(y_{i, i_0} - \frac{a_{i_0}^{(l)} + b_{i_0}^{(l)}}{2} \right) + \cos \left(-\frac{\pi}{2} \right) \left(y_{i, j_0} - \frac{a_{j_0}^{(l)} + b_{j_0}^{(l)}}{2} \right) + \frac{a_{i_0}^{(l)} + b_{i_0}^{(l)}}{2} \\
&= a_{i_0}^{(l)} + b_{i_0}^{(l)} - y_{i, i_0},
\end{aligned}$$

and $\tilde{y}_{ij} = y_{ij}$, for $j \neq i_0$ and $j \neq j_0$. As is readily apparent,

$$\left| \boldsymbol{\mu}_j^{(l)} - \tilde{\boldsymbol{\mu}}_j^{(l)} \right| = \begin{cases} \left| \boldsymbol{\mu}_j^{(l)} - \hat{\boldsymbol{\mu}}_j^{(l)} \right|, & j \neq i_0 \text{ and } j \neq j_0, \\ \left| \boldsymbol{\mu}_{j_0}^{(l)} - \hat{\boldsymbol{\mu}}_{j_0}^{(l)} \right|, & j = i_0, \\ \left| \boldsymbol{\mu}_{i_0}^{(l)} - \hat{\boldsymbol{\mu}}_{i_0}^{(l)} \right|, & j = j_0, \end{cases} \quad (19)$$

$$\left| \boldsymbol{\Sigma}_{jj}^{(l)} - \tilde{\boldsymbol{\Sigma}}_{jj}^{(l)} \right| = \begin{cases} \left| \boldsymbol{\Sigma}_{jj}^{(l)} - \hat{\boldsymbol{\Sigma}}_{jj}^{(l)} \right|, & j \neq i_0 \text{ and } j \neq j_0, \\ \left| \boldsymbol{\Sigma}_{j_0 j_0}^{(l)} - \hat{\boldsymbol{\Sigma}}_{j_0 j_0}^{(l)} \right|, & j = i_0, \\ \left| \boldsymbol{\Sigma}_{i_0 i_0}^{(l)} - \hat{\boldsymbol{\Sigma}}_{i_0 i_0}^{(l)} \right|, & j = j_0. \end{cases} \quad (20)$$

When $i = i_0$ and $j = j_0$,

$$\begin{aligned} & \left| \tilde{\boldsymbol{\Sigma}}_{i_0 j_0}^{(l)} \right| \\ &= \left| \frac{1}{n} \sum_{k=1}^n \left(y_{k, j_0} - \frac{1}{n} \sum_{h=1}^n y_{h, j_0} \right) \left(a_{i_0}^{(l)} + b_{i_0}^{(l)} - y_{k, i_0} - \frac{1}{n} \sum_{h=1}^n (a_{i_0}^{(l)} + b_{i_0}^{(l)} - y_{h, i_0}) \right) \right| \\ &= \left| \frac{1}{n} \sum_{k=1}^n - \left(y_{k, j_0} - \frac{1}{n} \sum_{h=1}^n y_{h, j_0} \right) \left(y_{k, i_0} - \frac{1}{n} \sum_{h=1}^n y_{h, i_0} \right) \right| \\ &= \left| \hat{\boldsymbol{\Sigma}}_{i_0 j_0}^{(l)} \right|. \end{aligned} \quad (21)$$

For other cases with $i \neq j$, it can also be similarly deduced that $\left| \tilde{\boldsymbol{\Sigma}}_{ij}^{(l)} \right| = \left| \hat{\boldsymbol{\Sigma}}_{ij}^{(l)} \right|$. Therefore, according to Eqs. (19)-(21), we have that the rotation transformation has no impact on the termination criterion (13). For Figure 2(a), the differences between the expectations and covariances of the two groups of particles and those of the uniform measure are

$$\begin{aligned} \left| \boldsymbol{\mu}^{(l)} - \hat{\boldsymbol{\mu}}^{(l)} \right| &= (0.25, 0), \\ \left| \boldsymbol{\Sigma}^{(l)} - \hat{\boldsymbol{\Sigma}}^{(l)} \right| &= \begin{pmatrix} \frac{5}{48} & 0 \\ 0 & \frac{1}{24} \end{pmatrix}. \end{aligned} \quad (22)$$

For Figure 2(b), the differences are

$$\begin{aligned} \left| \boldsymbol{\mu}^{(l)} - \hat{\boldsymbol{\mu}}^{(l)} \right| &= (0, 0.25), \\ \left| \boldsymbol{\Sigma}^{(l)} - \hat{\boldsymbol{\Sigma}}^{(l)} \right| &= \begin{pmatrix} \frac{1}{24} & 0 \\ 0 & \frac{5}{48} \end{pmatrix}. \end{aligned} \quad (23)$$

Obviously, Eqs. (22) and (23) merely involve a rearrangement of elements and thus does not affect the termination criterion (13). That is, the origin $\mathbf{0}$ in MSP is indistinctive, and there will be no such unreasonable phenomena of the star discrepancy in Figures 1 and 2.

4. Numerical experiments

This section conducts numerical experiments to test the numerical effects of DSP-mix and MSP compared with DSP. The first four distributions are from [4]. The L^2 relative error

$$\mathcal{E}_2[p] = \frac{\|p^{\text{num}}(\mathbf{x}) - p^{\text{ref}}(\mathbf{x})\|_2}{\|p^{\text{ref}}(\mathbf{x})\|_2} \quad (24)$$

is used to measure the accuracy, where $p^{\text{ref}}(\mathbf{x})$ is the reference solution and $p^{\text{num}}(\mathbf{x})$ is the numerical solution. We calculate the L^2 norm according to the partitioning \mathcal{P}_L ,

$$\|f(\mathbf{x})\|_2 \approx \sqrt{\sum_{l=1}^L f(\mathbf{x}_c)^2 |\Omega_l|}, \quad (25)$$

where \mathbf{x}_c is the center of Ω_l . The algorithm parameters are set as follows unless otherwise stated:

- DSP-mix: In Eq. (8), the parameter θ determining the level of refinement of the partition is set to 0.1. In Eq. (6), the parameter m specifying the number of candidate splitting points is set to 10;
- MSP: The tolerance parameters in Eq. (13) is $\epsilon_1 = 0.1, \epsilon_2 = 0.1, \epsilon_3 = 0.1$.

All simulations via C++ implementations run on the High-Performance Computing Platform of Peking University: 2*Intel Xeon E5-2697A-v4 (2.60GHz, 40MB Cache, 9.6GT/s QPI Speed, 16 Cores, 32 Threads), 256GB \times 16.

4.1. 2-D Gaussian

First we consider the 2-D Gaussian distribution [4],

$$\mathbf{x} \sim \mathcal{N}(\boldsymbol{\mu}, \boldsymbol{\Sigma}) \mathbb{1} \{ \mathbf{x} \in [0, 1]^2 \}, \quad (26)$$

where $\boldsymbol{\mu} = (0.5, 0.5)^T$ and $\boldsymbol{\Sigma} = [0.08, 0.02; 0.02, 0.02]$. Figure 3 shows the numerical solutions of the DSP, DSP-mix and MSP method. The proposed DSP-mix and MSP also have the ability to adaptively partition the computational domain, similar to DSP. They feature fine grids at positions where the probability density changes significantly and sparse grids in unimportant regions. Table 1 presents the L^2 relative error $\mathcal{E}_2[p]$ and running time of the three methods for the 2-D Gaussian example with the number of samples N . The errors of all three methods decrease as the number of samples N increases, and the errors of the three methods are comparable without significant order-of-magnitude gap. The running time of DSP-mix and MSP are similar and both runs approximately ten times faster than DSP.

Table 1. 2-D Gaussian: The L^2 relative error $\mathcal{E}_2[p]$ and running time in seconds (in parentheses) of the three methods under different sample sizes N .

| N | DSP | DSP-mix | MSP |
|-----------------|---------------------|--------------------|--------------------|
| 1×10^4 | 0.2747 (0.8109) | 0.2135 (0.0171) | 0.3218 (0.0161) |
| 1×10^5 | 0.1468 (3.3644) | 0.1303 (0.2074) | 0.1313 (0.1754) |
| 1×10^6 | 0.0968 (19.6516) | 0.0877 (2.2268) | 0.0888 (2.0470) |

4.2. 2-D Mixture of Gaussians

Next, we consider the 2-D mixture of Gaussians distribution [4],

$$\mathbf{x} \sim \frac{1}{2} \sum_{i=1}^2 \mathcal{N}(\boldsymbol{\mu}_i, \boldsymbol{\Sigma}_i) \mathbb{1} \{ \mathbf{x} \in [0, 1]^2 \}, \quad (27)$$

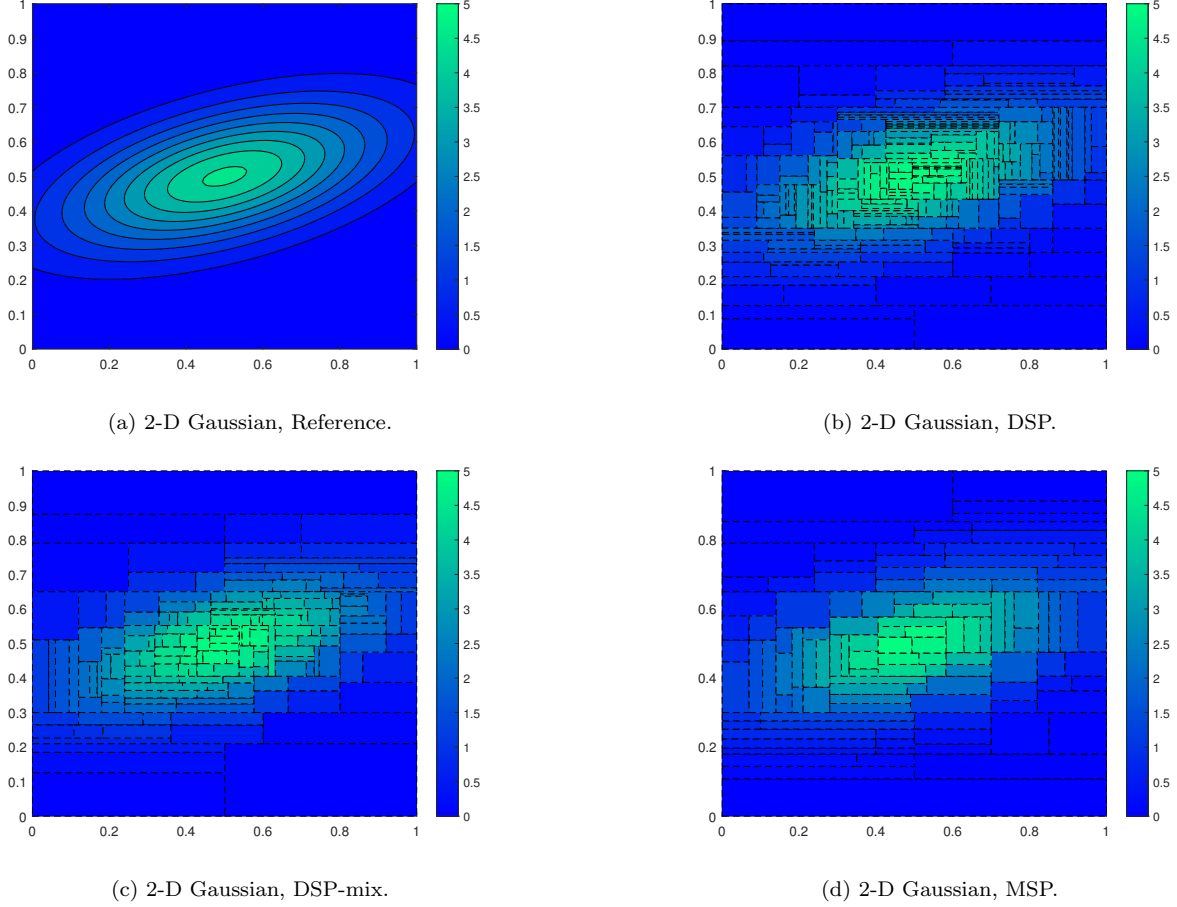
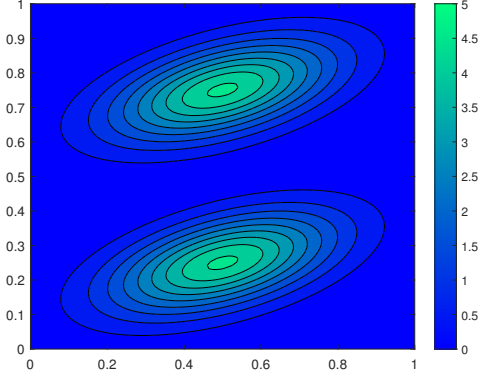


Figure 3. 2-D Gaussian: Numerical solutions produced by DSP-mix, MSP and DSP with $N = 1 \times 10^6$.

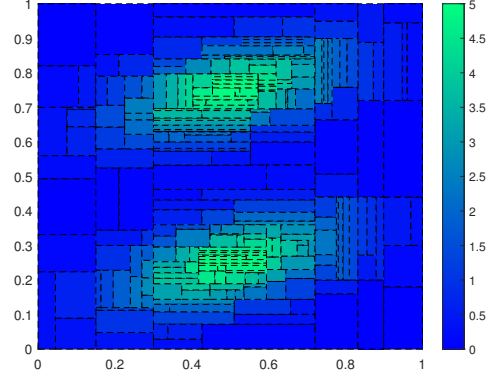
where $\boldsymbol{\mu}_1 = (0.5, 0.25)^T$, $\boldsymbol{\mu}_2 = (0.5, 0.75)^T$, $\boldsymbol{\Sigma}_1 = \boldsymbol{\Sigma}_2 = [0.04, 0.01; 0.01, 0.01]$. Figure 4 presents the numerical solutions of DSP, DSP-mix and MSP. All of them possess the capability to capture the distribution structure. Table 2 shows the L^2 relative errors $\mathcal{E}_2[p]$ and running time of the three methods for this example. Both DSP-mix and MSP can achieve approximately a tenfold speedup compared with DSP, while keeping the same accuracy.

Table 2. 2-D Mixture of Gaussians: The L^2 relative error $\mathcal{E}_2[p]$ and running time in seconds (in parentheses) of the three methods under different sample sizes N .

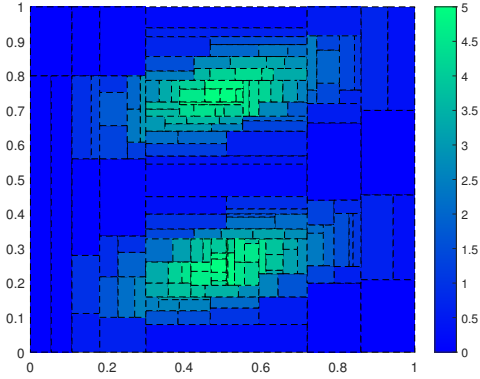
| N | DSP | DSP-mix | MSP |
|-----------------|---------------------|--------------------|--------------------|
| 1×10^4 | 0.2509 (0.8177) | 0.1754 (0.0163) | 0.2918 (0.0140) |
| 1×10^5 | 0.1067 (3.2465) | 0.0904 (0.2295) | 0.0988 (0.1795) |
| 1×10^6 | 0.0502 (19.6791) | 0.0349 (2.4601) | 0.0333 (2.0504) |



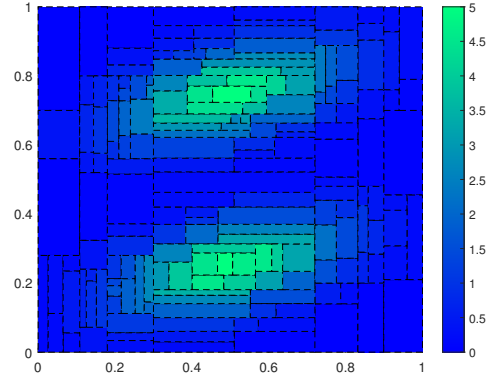
(a) 2-D Mixture of Gaussians, Reference.



(b) 2-D Mixture of Gaussians, DSP.



(c) 2-D Mixture of Gaussians, DSP-mix.



(d) 2-D Mixture of Gaussians, MSP.

Figure 4. 2-D Mixture of Gaussians: Numerical solutions produced by DSP-mix, MSP and DSP with $N = 1 \times 10^6$.

4.3. 2-D Mixture of Betas

In this numerical experiment, we test 2-D mixture of betas distribution [4],

$$\mathbf{x} \sim \frac{1}{3}(\text{beta}(2, 5) \text{beta}(5, 2) + \text{beta}(4, 2) \text{beta}(2, 4) + \text{beta}(1, 3) \text{beta}(3, 1)), \quad (28)$$

where $\text{beta}(\alpha, \beta)$ denotes beta distribution. Figure 5 displays the numerical visualizations of this example. Similar to the previous two examples, all three methods capture the main features of the distribution. Table 3 presents the L^2 relative errors $\mathcal{E}_2[p]$ and the running time of the three methods for this example respectively. The computational cost of DSP-mix and MSP is only about one-tenth of that of DSP, achieving an obvious speedup while maintaining the same precision.

4.4. d -D Mixtures of Gaussians

In this case, we test the d -D mixtures of Gaussians [4],

$$\mathbf{x}_i \sim \left(\sum_{i=1}^4 \alpha_i \mathcal{N}(\boldsymbol{\mu}_i, \boldsymbol{\Sigma}_i) \right), i = 1, \dots, N, \quad (29)$$

where $\boldsymbol{\alpha} = (0.4, 0.3, 0.2, 0.1)$, $\boldsymbol{\mu}_1 = 0.3\mathbb{1}$, $\boldsymbol{\mu}_2 = 0.4\mathbb{1}$, $\boldsymbol{\mu}_3 = 0.5\mathbb{1}$, $\boldsymbol{\mu}_4 = 0.6\mathbb{1}$, $\boldsymbol{\Sigma}_1 = 0.01\mathbf{I}$, $\boldsymbol{\Sigma}_2 = 0.02\mathbf{I}$, $\boldsymbol{\Sigma}_3 = 0.01\mathbf{I}$, $\boldsymbol{\Sigma}_4 = 0.02\mathbf{I}$. $\mathbb{1}$ is a $1 \times d$ all-one vector, and \mathbf{I} is a $d \times d$ identity matrix. Table 4 displays the numerical errors and computational costs of the three methods under different sample sizes N and dimensions d . The numerical results at different dimensions are still similar to those

Table 3. 2-D Mixture of Betas: The L^2 relative error $\mathcal{E}_2[p]$ and running time in seconds (in parentheses) of the three methods under different sample sizes N .

| N | DSP | DSP-mix | MSP |
|-----------------|---------------------|--------------------|--------------------|
| 1×10^4 | 0.3015 (0.8728) | 0.2469 (0.0162) | 0.3539 (0.0146) |
| 1×10^5 | 0.2069 (3.7691) | 0.2065 (0.2699) | 0.2066 (0.1808) |
| 1×10^6 | 0.1876 (24.7044) | 0.1821 (2.6406) | 0.1831 (2.0480) |

of the previous 2-D examples. The L^2 relative errors $\mathcal{E}_2[p]$ of the three density estimations are generally similar. However, in terms of running time, DSP-mix and MSP are significantly faster and can generally achieve a tenfold speedup. When the number of particles is relatively large (e.g. $N = 1 \times 10^6$), MSP exhibits greater speed advantages over DSP-mix. The underlying reason lies in the fact that the computational complexity of MSP scales linearly with the number of particles, in contrast to that of DSP-mix which is quadratic.

Table 4. d -D Mixtures of Gaussians: The L^2 relative error $\mathcal{E}_2[p]$ and running time in seconds (in parentheses) of the three methods under different sample sizes N and dimensions d .

| d | $N = 1 \times 10^4$ | | | $N = 1 \times 10^5$ | | | $N = 1 \times 10^6$ | | |
|-----|---------------------|--------------------|--------------------|---------------------|--------------------|--------------------|---------------------|--------------------|--------------------|
| | DSP | DSP-mix | MSP | DSP | DSP-mix | MSP | DSP | DSP-mix | MSP |
| 2 | 0.2340 (0.7537) | 0.2106 (0.0558) | 0.2489 (0.0133) | 0.0991 (2.6471) | 0.0723 (0.2065) | 0.0771 (0.1799) | 0.0415 (13.30) | 0.0231 (2.4144) | 0.0211 (2.1306) |
| 3 | 0.2966 (2.1429) | 0.2237 (0.0189) | 0.5455 (0.0187) | 0.1341 (7.3443) | 0.1268 (0.3405) | 0.1733 (0.2131) | 0.0773 (57.00) | 0.0663 (6.9713) | 0.0615 (2.823) |
| 4 | 0.3748 (3.0253) | 0.3108 (0.0208) | 0.7009 (0.0209) | 0.2211 (10.1659) | 0.2374 (0.3949) | 0.2715 (0.2517) | 0.1672 (67.59) | 0.1582 (9.184) | 0.1292 (3.4781) |
| 5 | 0.4864 (3.2468) | 0.4700 (0.0246) | 0.7270 (0.024) | 0.3530 (12.8835) | 0.4095 (0.4635) | 0.3734 (0.2914) | 0.2340 (82.18) | 0.3006 (10.94) | 0.2220 (4.3056) |
| 6 | 0.6148 (3.8357) | 0.7065 (0.0291) | 0.7792 (0.0282) | 0.4870 (15.8595) | 0.5746 (0.5347) | 0.4623 (0.3243) | 0.2966 (99.17) | 0.4578 (12.78) | 0.3227 (5.0615) |

4.5. d -D Mixtures of Betas

Finally we examine the d -D mixtures of betas,

$$\mathbf{x} \sim \frac{1}{3} \left(\prod_{j=1}^d \text{beta}(15, 5)(x_j) + \prod_{j=1}^d \text{beta}(10, 10)(x_j) + \prod_{j=1}^d \text{beta}(5, 15)(x_j) \right). \quad (30)$$

Table 5 displays the numerical errors and computational costs of the three methods for d -D mixtures of betas case. The errors of the three methods are comparable, all decreasing with the increase of the sample number N and increasing with the rise of the dimension d . When $N \geq 1 \times 10^5$, DSP-mix is approximately ten times faster than DSP, while MSP attains an acceleration approximately a hundred times. Figure 6 illustrates the influence of the parameters on the DSP-mix method and the

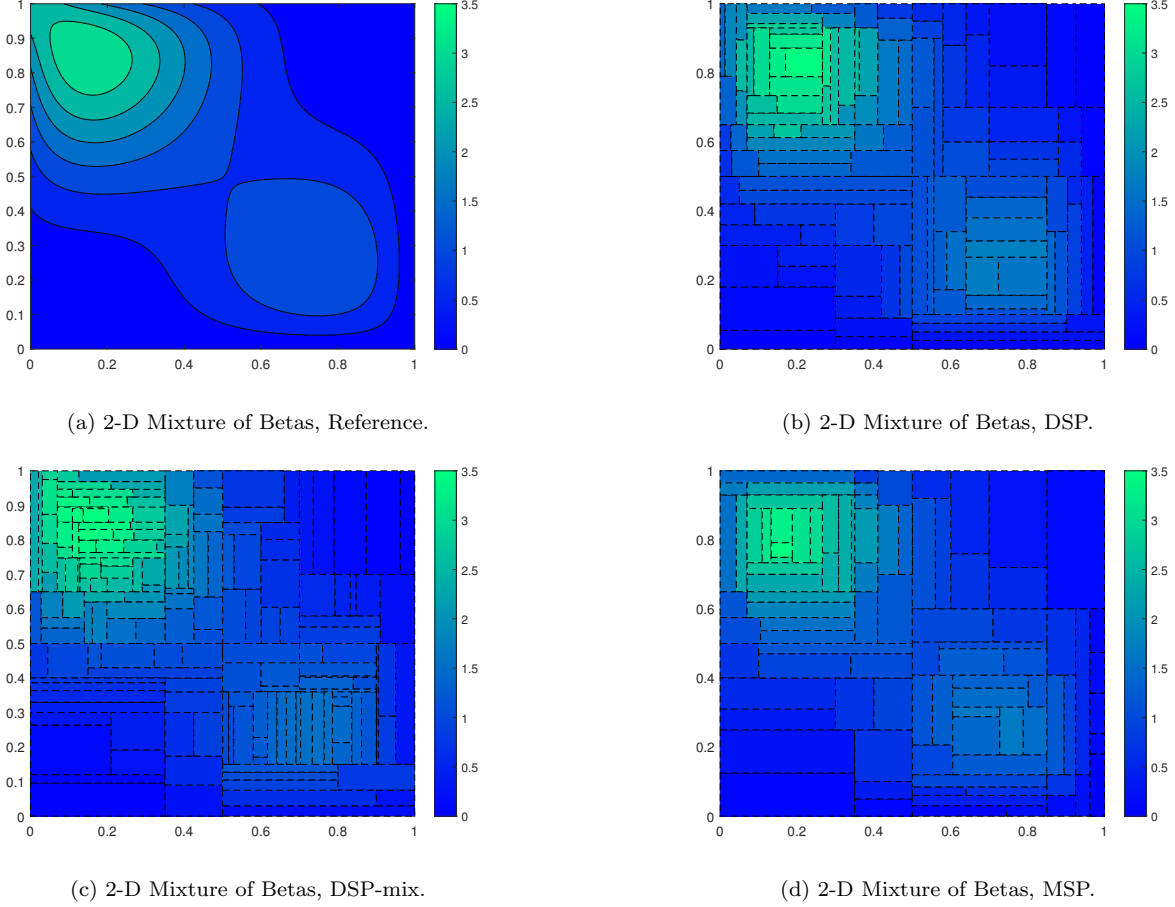


Figure 5. 2-D Mixture of Betas: Numerical solutions produced by DSP-mix, MSP and DSP with $N = 1 \times 10^6$.

MSP method. When θ , ϵ_1 , ϵ_2 and ϵ_3 decrease within a certain range, we can obtain finer partitioning and more accurate density estimation results. However, when these parameters are too small, the problem of overfitting will occur, and the error will instead increase. For the number of samples N , its increase will definitely make the solution more accurate.

5. Conclusion and discussion

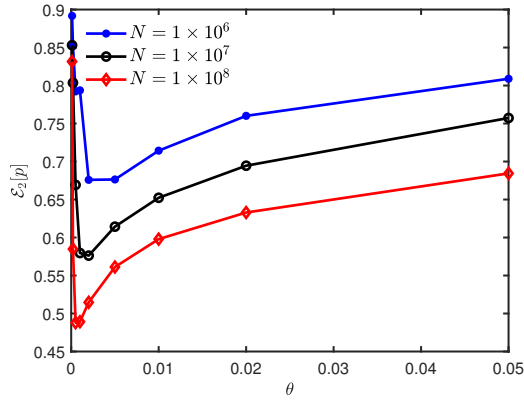
The main contributions of this work are to propose the DSP-mix and MSP methods. They still adopt the framework of the DSP method in [4] to learn a adaptive piecewise constant function to approximate the underlying probability density but respectively use mixture discrepancy and moments instead of star discrepancy as the uniformity measurements for observations. The mixture discrepancy and moments are easier to compute and theoretically maintain reflection invariance and rotation invariance, which are the shortcomings of the star discrepancy. Numerical experiments indicate that DSP-mix and MSP run approximately ten times faster than DSP while maintaining the same accuracy. There are still some issues worthy of further research, such as the quantitative error analysis of DSP-mix and MSP, the application to practical density estimation problems in higher dimensions, and more efficient uniformity measurement approaches.

Acknowledgement

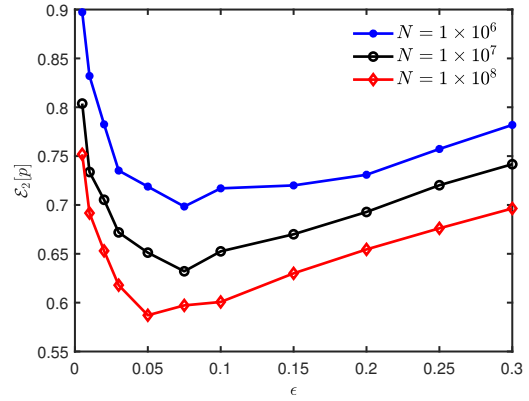
This research was supported by the National Natural Science Foundation of China (Nos. 12325112, 12288101) and the High-performance Computing Platform of Peking University.

Table 5. d -D Mixtures of Betas: The L^2 relative error $\mathcal{E}_2[p]$ and running time in seconds (in parentheses) of the three methods under different sample sizes N and dimensions d .

| d | $N = 1 \times 10^4$ | | | $N = 1 \times 10^5$ | | | $N = 1 \times 10^6$ | | |
|-----|---------------------|--------------------|--------------------|---------------------|--------------------|--------------------|----------------------|---------------------|--------------------|
| | DSP | DSP-mix | MSP | DSP | DSP-mix | MSP | DSP | DSP-mix | MSP |
| 2 | 0.2232 (0.9318) | 0.1954 (0.0165) | 0.2875 (0.0080) | 0.1077 (3.6159) | 0.0841 (0.2168) | 0.0846 (0.0494) | 0.0457 (17.1128) | 0.0274 (2.2811) | 0.0258 (0.5550) |
| 3 | 0.2790 (2.4086) | 0.2319 (0.0191) | 0.5789 (0.0173) | 0.1312 (8.7814) | 0.1241 (0.3537) | 0.1851 (0.0900) | 0.0818 (61.5023) | 0.0690 (7.0977) | 0.0634 (0.9356) |
| 4 | 0.3720 (3.2390) | 0.3224 (0.0223) | 0.7096 (0.0238) | 0.2318 (11.3189) | 0.2439 (0.4173) | 0.2908 (0.1315) | 0.1825 (76.6812) | 0.1694 (8.9815) | 0.1344 (1.2242) |
| 5 | 0.4646 (3.6802) | 0.4561 (0.0250) | 0.7782 (0.0314) | 0.3326 (14.6606) | 0.3838 (0.4746) | 0.3713 (0.1701) | 0.2926 (91.7739) | 0.2964 (10.3924) | 0.2209 (1.5386) |
| 6 | 0.5597 (4.2078) | 0.5910 (0.0280) | 0.7828 (0.0376) | 0.4555 (16.0885) | 0.5355 (0.5236) | 0.4423 (0.2034) | 0.4122 (104.2499) | 0.4311 (11.9599) | 0.3154 (1.8635) |



(a) The influence of θ on the error of DSP-mix.



(b) The influence of $\epsilon_1 = \epsilon_2 = \epsilon_3 = \epsilon$ on the error of MSP.

Figure 6. 10-D Mixtures of Betas: (a) When θ decreases within a certain range (0.002-0.05), the partitioning of DSP-mix becomes finer and the error will decrease. However, if θ is extremely small, the overfitting problem will occur. There are not enough samples in the sub-domain, leading to an increase in the error. When the number of samples N increases, a solution with higher accuracy can be obtained. (b) Let $\epsilon_1 = \epsilon_2 = \epsilon_3 = \epsilon$, and then observe how they affect the accuracy. Similarly, when the value of ϵ is extremely small (e.g. smaller than 0.05), the overfitting problem will arise in MSP. Nevertheless, an increase in the number of samples N will surely lead to higher accuracy.

References

- [1] B. W. Silverman, *Density Estimation for Statistics and Data Analysis*, Routledge, 2018.
- [2] S. Zámečník, I. Horová, S. Katina, K. Hasilová, An adaptive method for bandwidth selection in circular kernel density estimation, *Computational Statistics* 39 (2024) 1709–1728.
- [3] B. Yan, R. E. Caflisch, A Monte Carlo method with negative particles for Coulomb collisions, *Journal of Computational Physics* 298 (2015) 711–740.
- [4] D. Li, K. Yang, W. Wong, Density estimation via discrepancy based adaptive sequential partition, *Advances in Neural Information Processing Systems* (2016) 1099–1107.
- [5] Y. Xiong, S. Shao, Overcoming the numerical sign problem in the Wigner dynamics via adaptive particle annihilation, *SIAM Journal on Scientific Computing* 46 (2024) B107–B136.
- [6] J. Dick, F. Y. Kuo, I. H. Sloan, High-dimensional integration: the quasi-Monte Carlo way, *Acta Numerica* 22 (2013) 133–288.
- [7] F. Hickernell, A generalized discrepancy and quadrature error bound, *Mathematics of Computation* 67 (1998) 299–322.
- [8] K. Fang, M. Liu, H. Qin, Y. Zhou, *Theory and Application of Uniform Experimental Designs*, Springer, 2018.
- [9] P. Winker, K. T. Fang, Application of threshold-accepting to the evaluation of the discrepancy of a set of points, *SIAM Journal on Numerical Analysis* 34 (1997) 2028–2042.
- [10] M. Gnewuch, M. Wahlström, C. Winzen, A new randomized algorithm to approximate the star discrepancy based on threshold accepting, *SIAM Journal on Numerical Analysis* 50 (2012) 781–807.
- [11] Y. Zhou, K. Fang, J. Ning, Mixture discrepancy for quasi-random point sets, *Journal of Complexity* 29 (2013) 283–301.
- [12] P. Billingsley, *Probability and Measure*, John Wiley & Sons, 2012.
- [13] A. Gut, *Probability: a Graduate Course*, Springer, 2013.
- [14] R. J. Serfling, *Approximation Theorems of Mathematical Statistics*, John Wiley & Sons, Inc., 1980.
- [15] C. Kleiber, J. Stoyanov, Multivariate distributions and the moment problem, *Journal of Multivariate Analysis* 113 (2013) 7–18.
- [16] Z. Lei, S. Shao, Adaptive sampling accelerates the hybrid deviational particle simulations, arXiv preprint arXiv:2409.19584 (2024).